IEEE Access
Multidisciplinary | Rapid Review | Open Access Journal

Received December 13, 2018, accepted December 20, 2018, date of publication December 25, 2018,
date of current version January 11, 2019.

Digital Object Identifier 10.1109/ACCESS.2018.2889807

An Easily Fabricated Linear Piezoelectric Actuator Using Sandwich Longitudinal Vibrators With Four Driving Feet

WEISHAN CHEN, XINQI TIAN, KAILEI XUE, SHUO CHEN, AND HONGPENG YU
State Key Laboratory of Robotics and System, Harbin Institute of Technology, Harbin 150001, China

Corresponding author: Weishan Chen (cws@hit.edu.cn)

This work was supported in part by the National Natural Science Foundation of China under Grant 51475112 and Grant 51622502, and in part by the Foundation for Innovative Research Groups of the National Natural Science Foundation of China under Grant 51521003.

ABSTRACT A piezoelectric actuator using three sandwich longitudinal vibrators is proposed and tested. The two horizontal vibrators are parallel to each other and orthogonal to the vertical vibrator. The ends of the two horizontal vibrators serve as the four driving feet. The actuator has a simple fabricating process, which will shorten the period of fabrication. Two modes of the actuator are used to get the elliptical trajectories on the driving feet. The frequencies of the two modes are tuned to be about 21.60 kHz with modal analysis by the finite element method (FEM). The operating principle is also examined with transient analysis by FEM. A prototype is fabricated and its vibration characteristics are verified by using a scanning laser Doppler vibrometer. The prototype shows the best mechanical performance with the optimum working frequency and phase difference of 18.50 kHz and 60°, respectively. The typical output of the prototype is a no-load speed of 439.41 mm/s, a maximum thrust of 40 N, and a maximum power of 5.01 W at the voltage of 200 V_{P-P}. The mechanical characteristics of the prototype show that the exciting voltages can be used for the speed control due to the approximately linear relationship between them.

INDEX TERMS Linear piezoelectric actuator, resonant state, sandwich longitudinal vibrators, vibration test.

I. INTRODUCTION

Electromagnetism isolation, compact size, high resolution and self-lock at power off are the essential requirements for the actuators in the fields such as precision manufacturing [1]–[5], optical instruments [6]–[10], bioengineer and invasive surgery [11]–[15]. The piezo-actuated technology has been proved to be a promising candidate for these requirements. Piezoelectric actuators (PAs) use the inverse piezoelectric effect to convert the electrical energy from the power supply into the mechanical energy of stator, and usually the mechanical energy of stator is converted to the motion of the runner by friction coupling. The inverse piezoelectric effect directly transforms electrical energy into mechanical energy without magnetic field. And the friction coupling between the runner and the stator can make the piezoelectric actuator self-locking at power off.

The PAs can be classified into two types, resonant type [16]–[21] and non-resonant type [22]–[24], from the view of vibration state. Usually, the non-resonant type PAs are operated with the frequencies which are much lower than their first order resonance frequencies. And compliant mechanism are often utilized to amplify the output displacements of the piezoelectric elements [25], [26]. They can achieve high resolutions with a scale of nanometer easily [27]–[29], but their output speeds are limited [30], [31]. By contrast, the resonant type PAs can achieve long travel, high output speed and large thrust force, while their open-loop output resolutions are low [32]–[35]. The output resolution can be improved by close-loop control. For example, Kim *et al*. [36] proposed an ultrasonic linear motor with an optical linear encoder which achieved a maximum speed of 450 mm/s, a maximum thrust of 75 N, and a displacement resolution of 20 nm. Recently, Liu *et al.* [37] proposed a novel operating principle which uses the intermittent sine excitation signals to enhance the open-loop output displacement resolution, and a resolution of 0.21 μm was achieved by the prototype. However, the heating of the resonant type PA is serious when it works continuously. The change of output characteristics caused by temperature rise is a common challenge for the resonant type PA [38]–[40].

The resonant PAs can be categorized into standing wave type [16], [41]–[43], traveling wave type [17], [44], modes superposition type [19], [32], and resonant smooth impact type actuators [18], [21]. Oblique movements of driving feet are used to push the runner in standing wave piezoelectric actuators (SWPAs). For example, Zhang *et al.* [41] proposed a frog-shaped linear actuator with four feet, which obtained a speed of 287 mm/s and output thrust of 11.8 N. However, usually the SWPAs can only achieve unidirectional movements. Zhang *et al.* [42] proposed a SWPA with two vibrators which can achieve bi-directional movement at the cost of leaving parts of the piezoelectric elements unused. The actuator proposed by He *et al.* [43] also realizes bidirectional driving by carefully arranging the position of the driving feet and generating two different modes. However, the mechanical characteristics of the two directions are quite different, and it makes speed control more complicated.

Traveling waves are generated in the stators of the traveling wave piezoelectric actuators (TWPAs), and micro ellipse traces on the surface of stator are converted to macro movement of the runner by the friction between the stator and runner [45]–[47]. As the most developed resonant PAs, they have been put into commercial application in cameras. However, they are not suitable to serve as the linear actuators since traveling waves are difficult to be acquired in rods. Linear TWPAs have been proposed by Seemann [44] and Kurosawa *et al.* [48], but their structures are more complex than those of the rotary TWPAs.

The resonant smooth impact piezoelectric actuators (RSIPAs) are driven by the saw-tooth signals that lead to slow forward movements and rapid backward movements of the piezoelectric stators. Slips between the stator and runner are accumulated to achieve large travel and high speed motion by repeating these two successive movements at resonant frequency. The moving direction of RSIPAs can be reversed by changing the waveform of the exciting voltages. For example, Nishimura *et al.* [21] proposed a RSIPA using Langevin transducer, and a maximum speed of 0.28 m/s was achieved. RSIPAs can realize linear moving easily with the merits of simple structure and compact size, such as another RSIPA proposed by Yokose *et al.* [49]. It achieved a maximum speed about 125.7 mm/s with dimensions of 10 mm × 2 mm × 0.7 mm (length × width × thickness). However, wear of the RSIPAs is more serious than that the TWPAs and SWPAs, from the view of working principle.

Basing on the vibration superposition principle, elliptical trajectories on the driving feet are acquired by generating two modes with the same resonant frequency in the modes superposition piezoelectric actuators (MSPAs). Friction coupling between the driving feet and the runner turns the micro elliptical trajectories into the macro movement of the runner. The two modes used in MSPAs are generated by two sinusoidal signals with a certain phase difference, and exchanging of the signals will achieve the reversal of the output movement. Compared with the TWPAs, the MSPAs can easily achieve linear and rotary motions from the view of getting elliptical trajectories. For example, the two bending modes can be utilized in the linear and rotary actuators such as the actuators proposed by Liu *et al.* [32], [50]. Moreover, the problem of wear in MSPAs is also milder than that of the RSIPAs. However, RSIPAs have strict restrictions on their structural dimensions to ensure the resonant frequencies of vibrations approach each other. The RSIPAs have the merits of simple structures, compact sizes and flexible designs. The MSPAs can realize multi-DOF driving easily such as the actuators proposed by Liu *et al.* [51], Shi *et al.* [52], and Yang *et al.* [53].

In this work, a linear MSPA using bolt-clamped longitudinal vibrators with an easily fabricated structure is proposed. The influences of the structure parameters on the resonant frequencies are investigated. The vibration characteristics and mechanical performances are measured. The basic configuration and the operating principle of the actuator are discussed in Section II. Then, the actuator is analyzed with the model developed by the finite element method (FEM). Section IV gives the details of fabricating a prototype, the verifications of the vibration characteristics and the discussions of mechanical output characteristics through experiments.

II. STRUCTURE AND OPERATING PRINCIPLE

The proposed actuator consists of three bolt-clamped longitudinal vibrators, as shown in Figure 1(a). The horizontal and the vertical vibrators are arranged along X and Y directions, respectively. The four horns of the two horizontal vibrators serve as the driving feet, and the flange of the vertical vibrator is used to hold the actuator by the gripper. Figure 1(b) shows the polarizations of the PZT (lead zirconate titanate) plates and the voltages applied on the actuator. The ring shaped PZT plates are all polarized along their thickness directions. Forty-four pieces and thirty-two pieces of PZT plates are used in the horizontal and vertical vibrators, respectively. Copper electrodes and PZT plates are clamped in the vibrators one by one, the copper electrodes are used to apply the exciting voltages. The PZT plates in each vibrator are parallel connected together in electricity, and the voltage applied on each PZT plate is equal to the exciting voltage. The PZT plates of the two horizontal vibrators are carefully arranged so that they will vibrate inversely under the voltage V_A. The vertical vibrator is excited by the voltage V_B. The whole actuator has a symmetric structure, and Figure 1(c) shows a half cross-sectional view of the actuator. The PZT plates and the electrodes of the horizontal vibrators are clamped between the conical horns and the cube bolt, and the prepressures are applied through the threads on the cube bolt and horns. The horizontal vibrators are sleeved on the flange bolt through the holes of the cube blots together with the PZT plates, electrodes and horns. The PZT plates of the vertical vibrator are fastened by the nuts screwed on the flange bolt. The insulation cover is wound on the bolt to avoid short circuits between the excitation signals.

The cone-shaped horns used in the proposed actuator have a lower manufacture cost than the exponential horns which

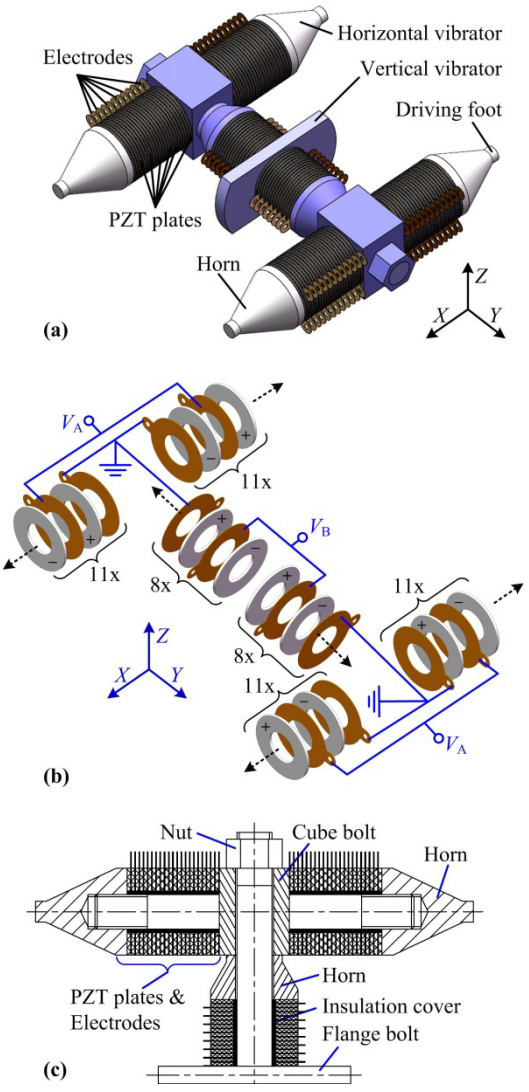

FIGURE 1. Structure of the proposed actuator: (a) axonometric view of the actuator (b) the polarizations of the PZT plates, (c) cross-sectional view of the actuator.

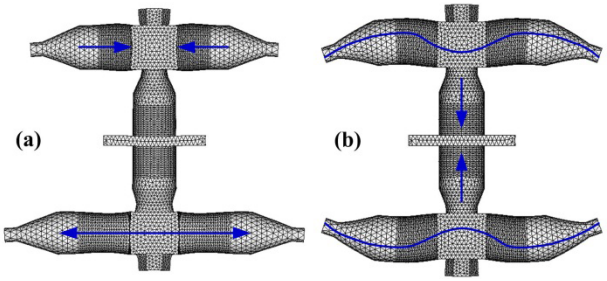

FIGURE 2. Vibration modes of the actuator: (a) mode-A, (b) mode-B.

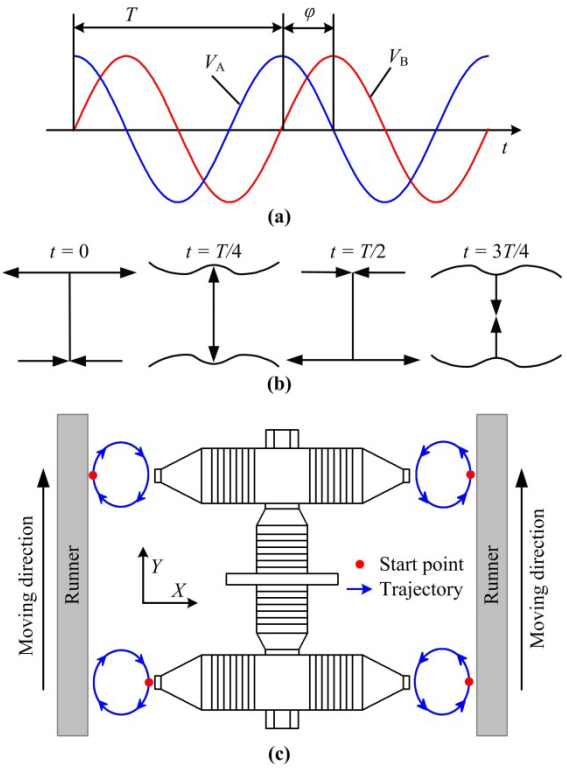

FIGURE 3. Operating principle of the proposed actuator: (a) the excitation signals, (b) deformations of the actuator in one period, (c) trajectories on the driving feet and working principle of the actuator.

are usually made by wire-electrode cutting. The structure of vertical vibrator also shortens the assembling period of the actuator. Details of the fabrication will be discussed in section IV.

The two modes shown in Figure 2 are used to form elliptical trajectories at the driving feet. The horizontal vibrators exhibit the first order longitudinal vibrations in mode-A. The horizontal vibrators oscillate with the third order transverse vibration while the vertical vibrator presents the first order longitudinal vibrations in mode-B.

Figure 3 shows the operating principle of the proposed piezoelectric linear actuator. The mode-A and mode-B are generated by the two sinusoidal voltages V_A and V_B simultaneously with the same frequency, as shown in Figure 3(a). The period, frequency and phase difference are labeled as T, f, and φ, respectively. In each period, the actuator will deform with the sequence shown in Figure 3(b). According to the superposition principle similar to Lissajous curve, elliptical trajectories will be obtained at the driving feet when V_A and V_B are applied on the actuator, as shown in Figure 3(c). The components of elliptical trajectories along X direction overcome the preload between the actuator and the runner while the components along Y direction push the runner into moving. The upper and lower side driving feet alternately drive the runner into movement. It is obvious that the runner can achieve bidirectional movement by changing the phase difference of the excitation signals V_A and V_B.

III. DESIGN AND ANALYSIS

In order to acquire elliptical trajectories efficiently, the frequencies of the mode-A and mode-B are tuned as close as possible. The design and analysis are accomplished by

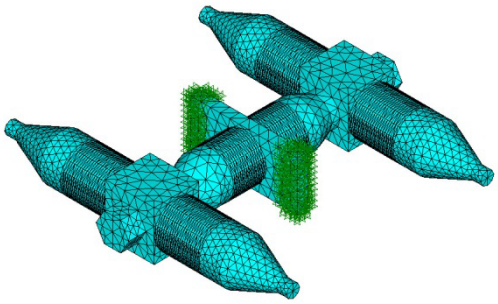

FIGURE 4. Finite element model of the proposed actuator.

finite element method (FEM) with the ANSYS software. The developed model is shown in Figure 4, and the flange of the actuator is under the fixed boundary condition. The copper electrodes and the insulation covers made by the polyvinyl chloride were neglected. The thickness of the electrodes was compensated by increasing the length of the horns. The flange blot, cube blots, nuts and the horn in the vertical vibrator are made by steel (mass density $\rho = 7.8 \times 10^3$ kg/m^3, Young's modulus $E = 2.06 \times 10^{11}$ N/m^2 and Poisson's ratio $\sigma = 0.3$). The material of the horns in horizontal vibrators is duralumin alloy ($\rho = 2.81 \times 10^3$ kg/m^3, $E = 7.2 \times 10^{10}$ N/m^2 and Poisson's ratio $\sigma = 0.33$). The material of the PZT ceramic is PZT-4, whose physical parameters are as follows:

$$d = \begin{bmatrix} 0 & 0 & 0 & 0 & 5 & 0 \\ 0 & 0 & 0 & 5 & 0 & 0 \\ -1.6 & -1.6 & 3.3 & 0 & 0 & 0 \end{bmatrix} \times 10^{-10}\text{C/N}$$

$$[C^E] = \begin{bmatrix} 14.3 & 7.85 & 7.85 & 0 & 0 & 0 \\ 7.85 & 14.3 & 7.85 & 0 & 0 & 0 \\ 7.85 & 7.85 & 11.5 & 0 & 0 & 0 \\ 0 & 0 & 0 & 2.6 & 0 & 0 \\ 0 & 0 & 0 & 0 & 2.45 & 0 \\ 0 & 0 & 0 & 0 & 0 & 2.45 \end{bmatrix}$$

$$[\varepsilon^T] = \begin{bmatrix} 8.1 & 0 & 0 \\ 0 & 8.1 & 0 \\ 0 & 0 & 6.7 \end{bmatrix} \times 10^{-9}\ \text{F/m}$$

$$\rho = 7.6 \times 10^3 \text{kg/m}^3$$

where d, c^E, ε^T and ρ are the piezoelectric constant matrix, the stiffness matrix at constant electric field, the dielectric matrix at constant stress and the mass density, respectively.

Seven structural parameters shown in Figure 5 are selected to investigate their influence on the frequencies of mode-A and mode-B. They are used to accomplish the mode degeneracy in design, and they provided guide for frequency adjustment after the fabrication of the prototype. Modal analyses are carried out with different simulation values of the structural parameters. Each simulation value C of structural parameters is decided by the initial value P, basic increment δ and gain factor G with the equation $C = P + G\delta$, as listed in Table 1. The results are shown in Figure 6 and Figure 7.

The frequencies of mode-A and mode-B are labeled f_A and f_B, respectively. It can be seen in Figure 6 that L_2 and

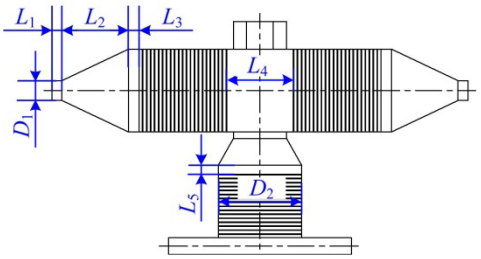

FIGURE 5. Structural parameters used in the mode degeneracy.

TABLE 1. Initial values and basic increments of the structure parameters.

Structure parameter	Initial value P (mm)	Basic increment δ (mm)
D_1	7	0.2
D_2	22	0.5
L_1	5	0.2
L_2	20	1
L_3	10	0.5
L_4	24	0.5
L_5	8	0.5

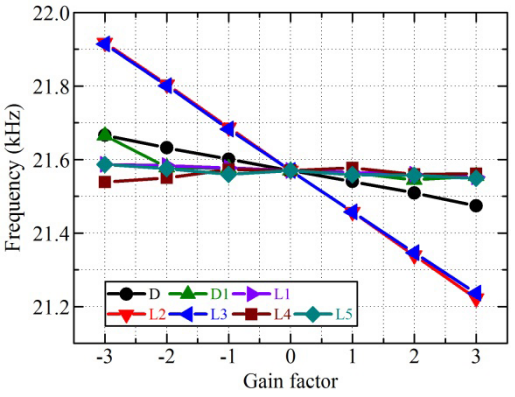

FIGURE 6. Frequencies of mode-A under different gain factors of structural parameters.

L_3 have more obvious effect on f_A than the other parameters. Figure 7 indicates that L_2, L_3, and D_1 have stronger influence on f_B, than the other parameters. It is notable that D_1 and L_2 affect f_B oppositely. Thus L_2, L_3, and D_1 are selected to tune the frequencies of the two modes coarsely, while L_1, L_4, L_5 and D_2 are trimmed to achieve accurate match of the two frequencies. The working frequency of the proposed actuator is designed as 21.60 kHz with the final dimensions shown in Figure 8. Transient analysis is used to validate the working principle of the proposed actuator. V_A and V_B, with the same frequency of 20.60 kHz, voltage of 200 V_{P-P} (volts with peak to peak value), and phase difference of 90° are applied on the actuator. The motion trajectories of the four driving feet are the same, one of them are plotted in Figure 9.

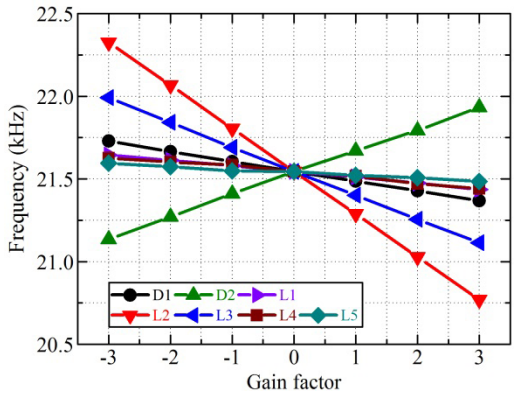

FIGURE 7. Frequencies of mode-B under different gain factors of structural parameters.

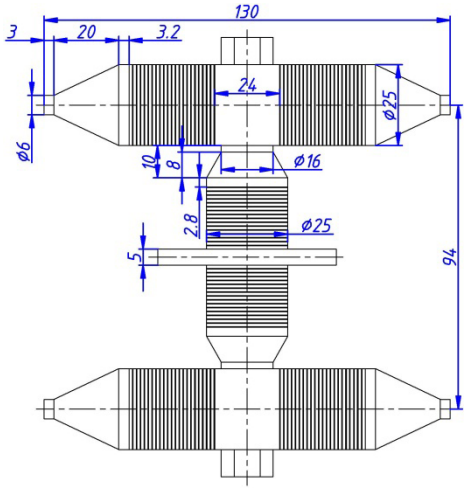

FIGURE 8. Final structural parameters of the actuator (unit: mm).

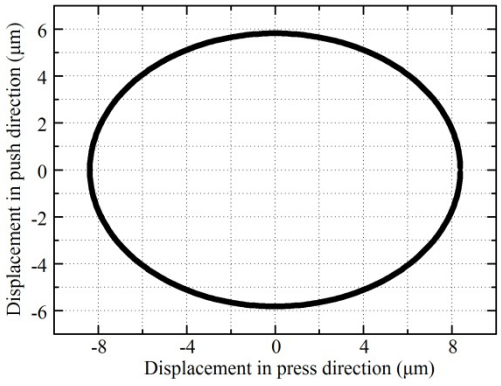

FIGURE 9. Motion trajectory of driving foot by transits analysis.

It can be found that the elliptical trajectories are obtained on the driving feet. The vibration amplitudes in the pressing direction (X direction) and the pushing direction (Y direction) are 4.19 μm and 2.91 μm, respectively.

IV. FABRICATION AND EXPERIMENTS

The actuator has an easy fabrication process that only needs three steps after the machining of the components, as shown

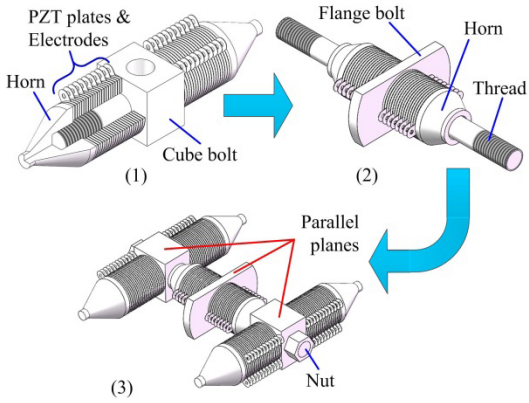

FIGURE 10. The fabrication process of the prototype.

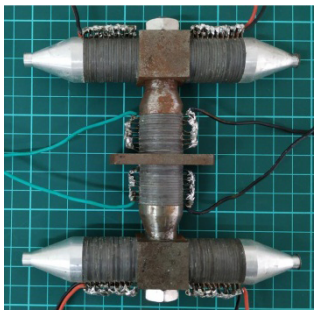

FIGURE 11. The photo of the prototype (unit of the grids: 1cm).

in Figure 10. Firstly, the two horizontal vibrators were assembled. The PZT plates and electrodes were clamped between the cube bolt and the horns with a pre-press load of 30 MPa. The pre-press load was applied with a torque wrench and a drill chuck clamping the cylindrical surface of the horn. Secondly, the vertical vibrator was assembled. The PZT plates, electrodes and the horizontal vibrators were sleeved on the flange bolt. Finally, the actuator was placed on a magnetic platform of a surface grinder with the three parallel planes on it to ensure that the three vibrators were in the same location as design. And the nuts were screwed with a torque wrench by which pre-press loads of 30 MPa were maintained on the PZT plates. The proposed prototype is shown in Figure 11. Compared with the conventional fabrication process of the blot-clamped linear piezoelectric actuators proposed by Liu *et al.* [54], [55] and Zhang *et al.* [41], the conical horns of the proposed actuator have the merits of simple structure and easy manufacturing. Furthermore, all the components do not need machining during the whole assembly process, which simplifies the fabrication process and shortens the fabrication period.

The vibration characteristics of the prototype were measured with a scanning laser Doppler vibrometer (PSV-400-M2, Polytec, Germany). Area-I and Area-II shown in Figure 12 were scanned to measure the vibration characteristics of the mode-A and mode-B respectively. Area-I contained the side surface of two driving feet, and Area-II indicated the side surface of the horizontal vibrator.

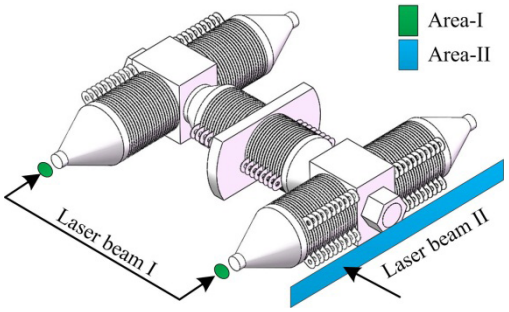

FIGURE 12. Methods of the vibration scans.

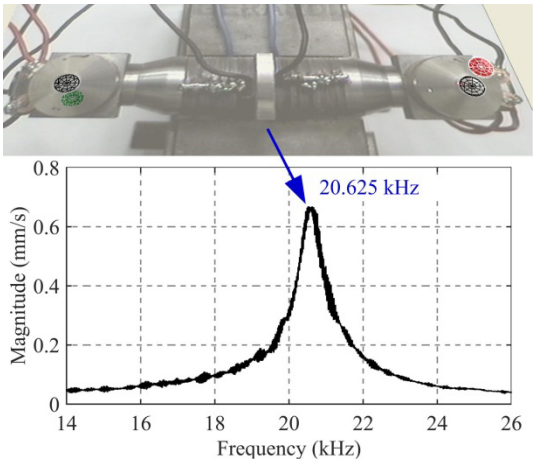

FIGURE 13. Vibration scanning result of the mode-A.

Figure 13 shows that the two driving feet vibrated in longitudinal direction opposite with the same magnitude at the resonant frequency of 20.625 kHz. Transverse vibration of the horizontal vibrator with four wave nodes was measured at the resonant frequency of 19.422 kHz, as illuminated in Figure 14. The scanning results shown in Figure 13 and Figure 14 verified the two modes designed in operating principle. The difference between the measured resonant frequencies of mode-A and mode-B could be diminished by lengthening L_5 and shortening L_2, according to the sensitivities of resonant frequencies to the structural parameters. The discrepancies between results calculated by FEM and the measured results might be caused by the modeling, machining and assembling errors of the prototype.

The mechanical output performance was measured with the experiment setups shown in Figure 15. The proposed actuator was fixed on the base by the clamper. The runner (weight of 2.6 kg) held on the guider was pressed on the driving feet with the bolt. And the preloads could be adjusted by screwing the blot through the bracket-shaped nut fixed on the base. The magnetic grating ruler (Model: MB200/1, SIKO, Germany) bonded on the runner and the magnetic sensor (Model: MSK200/1-0085, SIKO, Germany) were utilized to measure the output speed. The thrust force was applied by the weight linked with the runner through the string and

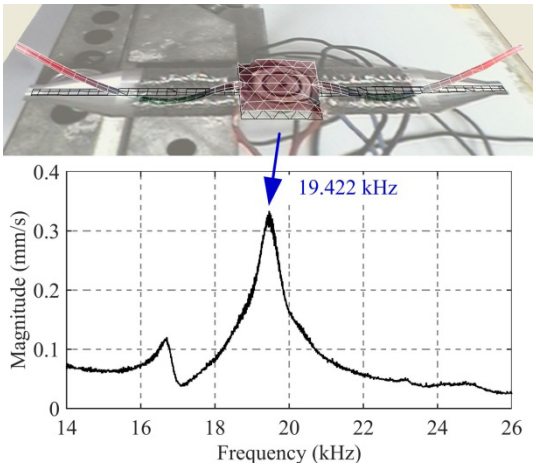

FIGURE 14. Vibration scanning result of the mode-B.

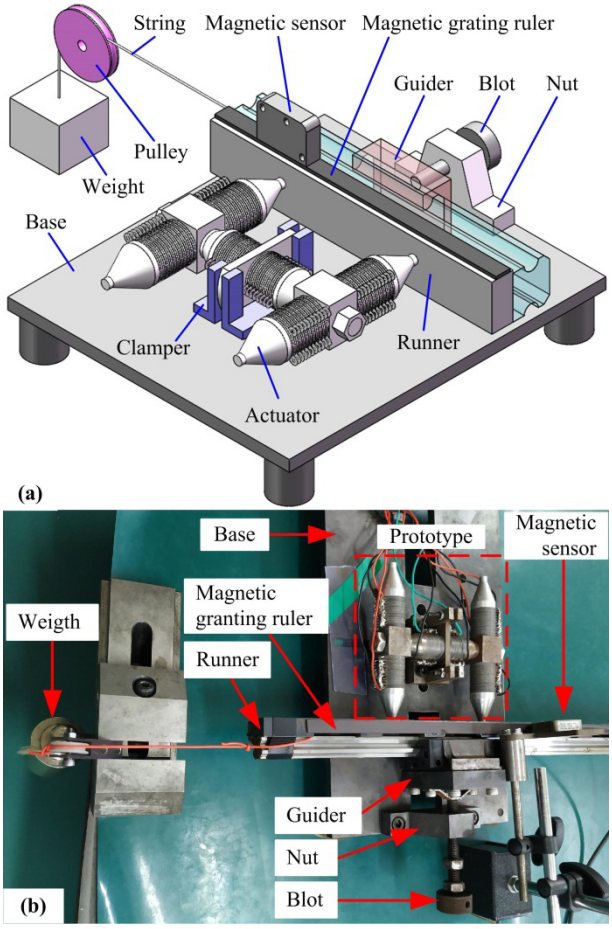

FIGURE 15. Experiment setups for mechanical output performance: (a) method, (b) real instruments.

the pulley. A quadrature counter (Model: PCI2394, ART Technology, China) and a personal computer were used to acquire and process the signals from the magnetic sensor. The two excition voltages were supplied by a ultrasonic power supply (Model: QD-8A, Strivertech, China). The tests for

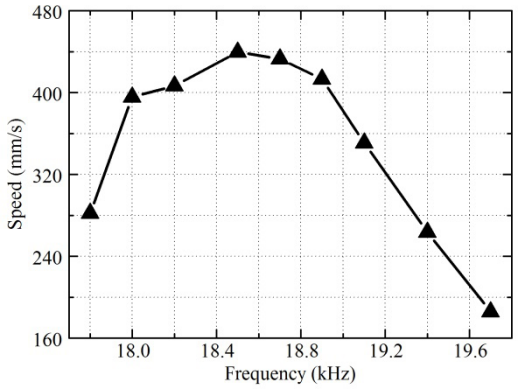

FIGURE 16. Plot of the speed versus the frequency.

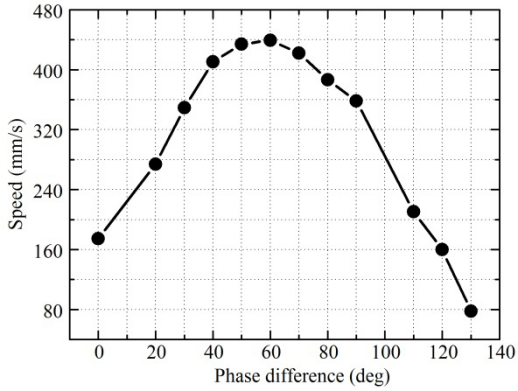

FIGURE 17. Plot of the speed versus the phase difference.

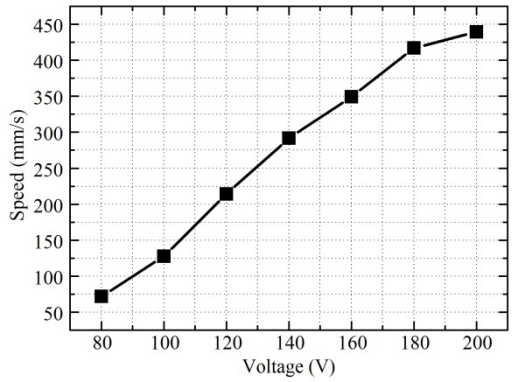

FIGURE 18. Plot of the speed versus the exciting voltage.

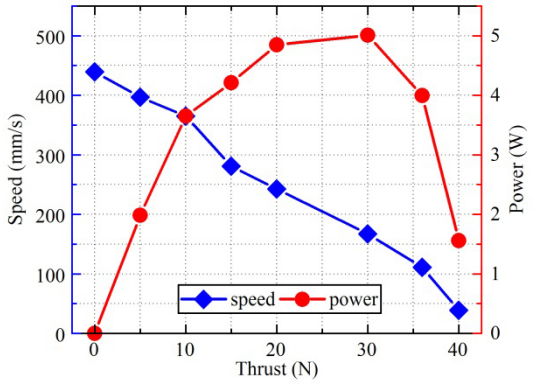

FIGURE 19. Plots of the speed and the output power versus the thrust.

mechanical performance were carried out in indoors with an ambient temperature about 25°C.

Firstly, the no-load output speeds of the prototype were measured under different frequencies. The pre-load was set as 300 N during the measurement, while the voltages and the phase difference of the excitation signals were 200 V_{p-p} and 60°, respectively. It can be found in Figure 16 that the prototype reached the peak speed of 439.41 mm/s at the frequency of 18.50 kHz, and this frequency is label as the optimum working frequency. The discrepancies between the optimum working frequency and the resonance frequencies measured by the Doppler vibrometer might be generated by the constraint conditions of the flange and the preload between the driving feet and the runner.

Secondly, the optimum working phase difference was searched. The no-load output speeds of the prototype were tested under different phase differences with the condition that the pre-load, the voltages and frequency of the excitation were 300 N, 200 V_{p-p} and 18.50 kHz, respectively. The prototype reached a maximum speed of 439.41 mm/s at the optimum working phase difference of 60°, as shown in Figure 17. Besides, the speed-phase characteristic curve of the prototype was almost symmetrical about 60°.

Thirdly, the effect of exciting voltages on output speed was investigated with the pre-load of 300 N, the thrust force of zero, the optimum working frequency and the optimum working phase difference. The speed almost linearly depended on the voltages of the excitation signals in the range from 80 V_{p-p} to 200 V_{p-p}, as shown in Figure 18. And this indicates that the voltage is very suitable for the speed control. It is noteworthy that the minimum stable output speed was 72.01 mm/s at the voltage of 80 V_{p-p}.

Finally, the output thrust force of the prototype was measured. The pre-load, frequency, phase difference and voltages of the excitation signals were set as 300 N, 18.5 kHz, 60° and 200 V_{p-p}, respectively. The output speed decreased with the increasing of thrust force, as shown in Figure19. The maximum thrust force was about 40 N. Moreover, the prototype reached a peak mechanical output power of 5.01 W at the thrust of 30 N with the speed of 166.7 mm/s.

The proposed actuator has advantages in output speed and thrust, compared with linear actuator proposed by Suzuki *et al.* [34], which achieved the 3 N on the maximum thrust force and 112 mm/s on the maximum speed. Tenzer and Ben Mrad [56] have proposed an inchworm like actuator with four driving feet that has achieved a maximum thrust of 150 N and a speed of 20 mm/s. The proposed actuator in this work has a similar profile and working principle. Although the output thrust in this work is only 26% of that of the actuator proposed by Tenzer and Ben Mrad [56], yet the out speed is 21.9 times as fast as that one. Compared with the easy fabricated liner actuator working in resonant

TABLE 2. Comparison between the proposed piezoelectric actuator and the previous works.

Actuator	Voltage	Maximum speed (mm/s)	Maximum thrust (N)	Speed per V_{RMS} ($mm \cdot s^{-1}/V_{RMS}$)	Thrust per V_{RMS} (N/V_{RMS})
This work	200 V_{P-P}	439.41	40	6.21	0.57
Reference [54]	200 V_{RMS}	1160	20	5.8	0.1
Reference [55]	200 V_{RMS}	854	40	4.27	0.2
Reference [58]	200 V_{RMS}	600	20	3	0.1
Reference [59]	100 V_{RMS}	750	16	7.5	0.16
Reference [60]	500 V_{P-P}	384	90	2.17	0.51

state that proposed by Chen *et al.* [57], whose maximum speed and thrust were 310 mm/s and 2.35 N, the actuator proposed in this work has the obvious merit of large output thrust force. Comparisons between the proposed actuator and the previous resonant type piezoelectric actuators using the longitudinal vibrators are shown in the Table 2. It is noteworthy that the sinusoidal voltages applied on these actuators are expressed by different statistical parameters. For the same sinusoidal signal, voltage expressed by peak-peak value (V_{P-P}) is 2.828 times that expressed by root-mean-square value (V_{RMS}). It can be found that the proposed actuator has advantages in the output speed per volt or thrust per volt.

V. CONCLUSION

A linear piezoelectric actuator working in resonant state was proposed and its mechanical output performances were investigated. Three blot-clamped longitudinal vibrators with conical horns were integrated orthogonally. The structure of actuator made the fabrication process easy and short. FEM models were developed to accomplish the modal degeneracy and verify the operating principle of the proposed actuator. The working frequency of the actuator was designed as 20.6 kHz. The vibration characteristics of the two modes adopted in the actuator were verified with a laser Doppler vibrometer by scanning a prototype. The mechanical characteristics of the prototype were measured, and the optimum working frequency and the optimum working phase difference were 18.50 kHz and 60°, respectively. The prototype achieved a maximum speed of 439.41 mm/s, a maximum thrust about 40 N, and a maximum power of 5.01 W at the exciting voltages of 200 V_{P-P}. It was founded that the output speed nearly depended on the exciting voltages. The actuator may achieve better mechanical performance by using a much powerful power supply. Future works will focus on improving the low speed stability of the proposed actuator with close-loop control.

REFERENCES

[1] C. Ma, E. Shamoto, T. Moriwaki, and L. Wang, "Study of machining accuracy in ultrasonic elliptical vibration cutting," *Int. J. Mach. Tools Manuf.*, vol. 44, nos. 12–13, pp. 1305–1310, 2004.

[2] P. Guo and K. F. Ehmann, "Development of a tertiary motion generator for elliptical vibration texturing," *Precis. Eng.*, vol. 37, no. 2, pp. 364–371, 2013.

[3] Z. Zhu, S. To, G. Xiao, K. F. Ehmann, and G. Zhang, "Rotary spatial vibration-assisted diamond cutting of brittle materials," *Precis. Eng.*, vol. 44, pp. 211–219, Apr. 2016.

[4] X. Zhou, C. Zuo, Q. Liu, R. Wang, and J. Lin, "Development of a double-frequency elliptical vibration cutting apparatus for freeform surface diamond machining," *Int. J. Adv. Manuf. Technol.*, vol. 87, nos. 5–8, pp. 2099–2111, 2016.

[5] Y. Gu, Y. Zhou, J. Lin, M. Lu, C. Zhang, and X. Chen, "Design, analysis, and testing of a flexure-based vibration-assisted polishing device," *AIP Adv.*, vol. 8, no. 5, p. 055113, 2018.

[6] X. Wang, V. Pommier-Budinger, A. Reysset, and Y. Gourinat, "Simultaneous compensation of hysteresis and creep in a single piezoelectric actuator by open-loop control for quasi-static space active optics applications," *Control Eng. Pract.*, vol. 33, pp. 48–62, Dec. 2014.

[7] W. Liu *et al.*, "A tip–tilt–piston micromirror with a double S-shaped unimorph piezoelectric actuator," *Sens. Actuator A, Phys.*, vol. 193, pp. 121–128, Apr. 2013.

[8] K. H. Koh, T. Kobayashi, and C. Lee, "A 2-D MEMS scanning mirror based on dynamic mixed mode excitation of a piezoelectric PZT thin film S-shaped actuator," *Opt. Express*, vol. 19, no. 15, pp. 13812–13824, 2011.

[9] D. Do, H. Yoo, and D.-G. Gweon, "Fiber-optic raster scanning two-photon endomicroscope using a tubular piezoelectric actuator," *J. Biomed. Opt.*, vol. 19, no. 6, p. 6, 2014, Art. no. 066010.

[10] W. Zhu, L. Bian, Y. An, G. Chen, and X. Rui, "Modeling and control of a two-axis fast steering mirror with piezoelectric stack actuators for laser beam tracking," *Smart Mater. Struct.*, vol. 24, no. 7, 2015, Art. no. 075014.

[11] Q. Zhou, K. H. Lam, H. Zheng, W. Qiu, and K. K. Shung, "Piezoelectric single crystal ultrasonic transducers for biomedical applications," *Prog. Mater. Sci.*, vol. 66, pp. 87–111, Jun. 2014.

[12] O. Ferhanoglu, M. Yildirim, K. Subramanian, and A. Ben-Yakar, "A 5-mm piezo-scanning fiber device for high speed ultrafast laser microsurgery," *Biomed. Opt. Express*, vol. 5, no. 7, pp. 2023–2036, Jul. 2014.

[13] F. Abella, J. de Ribot, G. Doria, F. Duran-Sindreu, and M. Roig, "Applications of piezoelectric surgery in endodontic surgery: A literature review," *J. Endodontics*, vol. 40, no. 3, pp. 325–332, 2014.

[14] G. Wang and Q. Xu, "Design and precision position/force control of a piezo-driven microinjection system," *IEEE/ASME Trans. Mechatronics*, vol. 22, no. 4, pp. 1744–1754, Aug. 2017.

[15] W. Shang, D. Li, H. Lu, T. Fukuda, and Y. Shen, "Less-invasive non-embedded cell cutting by nanomanipulation and vibrating nanoknife," *Appl. Phys. Lett.*, vol. 110, no. 4, p. 043701, 2017.

[16] L. Wang, J. Liu, Y. Liu, X. Tian, and J. Yan, "A novel single-mode linear piezoelectric ultrasonic motor based on asymmetric structure," *Ultrasonics*, vol. 89, pp. 137–142, Sep. 2018.

[17] P. Hagedorn and J. Wallaschek, "Travelling wave ultrasonic motors, Part I: Working principle and mathematical modelling of the stator," *J. Sound Vib.*, vol. 155, no. 1, pp. 31–46, 1992.

[18] T. Morita, H. Murakami, T. Yokose, and H. Hosaka, "A miniaturized resonant-type smooth impact drive mechanism actuator," *Sens. Actuator A, Phys.*, vol. 178, pp. 188–192, May 2012.

[19] M. K. Kurosawa, O. Kodaira, Y. Tsuchitoi, and T. Higuchi, "Transducer for high speed and large thrust ultrasonic linear motor using two sandwich-type vibrators," *IEEE Trans. Ultrason., Ferroelect., Freq. Control*, vol. 45, no. 5, pp. 1188–1195, Sep. 1998.

[20] D. Xu, Y. Liu, J. Liu, and W. Chen, "A bonded type ultrasonic motor using the bending of a crossbeam," *IEEE Access*, vol. 4, pp. 1109–1116, 2016.

[21] T. Nishimura, H. Hosaka, and T. Morita, "Resonant-type smooth impact drive mechanism (SIDM) actuator using a bolt-clamped Langevin transducer," *Ultrasonics*, vol. 52, no. 1, pp. 75–80, 2012.
[22] Y. Liu, L. Wang, Z. Gu, Q. Quan, and J. Deng, "Development of a two-dimensional linear piezoelectric stepping platform using longitudinal-bending hybrid actuators," *IEEE Trans. Ind. Electron.*, vol. 66, no. 44, pp. 3030–3040, Apr. 2019, doi: 10.1109/TIE.2018.2842730.
[23] J. Deng, Y. Liu, J. Liu, D. Xu, and Y. Wang, "Development of a planar piezoelectric actuator using bending-bending hybrid transducers," *IEEE Trans. Ind. Electron.*, Oct. 2018, doi: 10.1109/TIE.2018.2873123.
[24] L. Wang, D. Chen, T. Cheng, P. He, X. Lu, and H. Zhao, "A friction regulation hybrid driving method for backward motion restraint of the smooth impact drive mechanism," *Smart Mater. Struct.*, vol. 25, no. 8, 2016, Art. no. 085033.
[25] T.-P. Dao and S.-C. Huang, "Optimization of a two degrees of freedom compliant mechanism using Taguchi method-based grey relational analysis," *Microsyst. Technol.*, vol. 23, no. 10, pp. 4815–4830, 2017.
[26] T.-P. Dao and S.-C. Huang, "Design and multi-objective optimization for a broad self-amplified 2-DOF monolithic mechanism," *Sādhanā*, vol. 42, no. 9, pp. 1527–1542, 2017.
[27] G.-Y. Gu, L.-M. Zhu, C.-Y. Su, H. Ding, and S. Fatikow, "Modeling and control of piezo-actuated nanopositioning stages: A survey," *IEEE Trans. Autom. Sci. Eng.*, vol. 13, no. 1, pp. 313–332, Jan. 2016.
[28] G. Y. Gu, L. M. Zhu, C. Y. Su, H. Ding, and S. Fatikow, "Proxy-based sliding-mode tracking control of piezoelectric-actuated nanopositioning stages," *IEEE/ASME Trans. Mechatronics*, vol. 20, no. 4, pp. 1956–1965, Aug. 2015.
[29] Q. Xu, "Digital sliding mode prediction control of piezoelectric micro/nanopositioning system," *IEEE Trans. Control Syst. Technol.*, vol. 23, no. 1, pp. 297–304, Oct. 2015.
[30] D. Xu, Y. Liu, S. Shi, J. Liu, W. Chen, and L. Wang, "Development of a nonresonant piezoelectric motor with nanometer resolution driving ability," *IEEE/ASME Trans. Mechatronics*, vol. 23, no. 1, pp. 444–451, Feb. 2018.
[31] Q. Su, Y. Liu, L. Wang, J. Deng, and H. Li, "A three-dimensional piezoelectric nanopositioner using a sandwich transducer," *Ceramics Int.*, vol. 44, pp. S108–S111, Nov. 2018, doi: 10.1016/j.ceramint.2018.08.226.
[32] Y. Liu, W. Chen, J. Liu, and X. Yang, "A high-power linear ultrasonic motor using bending vibration transducer," *IEEE Trans. Ind. Electron.*, vol. 60, no. 11, pp. 5160–5166, Nov. 2013.
[33] A. Iula and M. Pappalardo, "A high-power traveling wave ultrasonic motor," *IEEE Trans. Ultrason., Ferroelectr., Freq. Control*, vol. 53, no. 7, pp. 1344–1351, Jul. 2006.
[34] M. Suzuki, H. Hosaka, and T. Morita, "Resonant-type smooth impact drive mechanism actuator with two Langevin transducers," *Adv. Robot.*, vol. 26, nos. 3–4, pp. 277–290, 2012.
[35] S. Park and S. He, "Standing wave brass-PZT square tubular ultrasonic motor," *Ultrasonics*, vol. 52, no. 7, pp. 880–889, 2012.
[36] W.-S. Kim, C.-H. Yun, and S.-K. Lee, "Nano positioning of a high power ultrasonic linear motor," *Jpn. J. Appl. Phys.*, vol. 47, no. 7R, pp. 5687–5692, 2008.
[37] J. Liu, Y. Liu, L. Zhao, D. Xu, W. Chen, and J. Deng, "Design and experiments of a single-foot linear piezoelectric actuator operated in stepping mode," *IEEE Trans. Ind. Electron.*, vol. 65, no. 10, pp. 8063–8071, Jan. 2018.
[38] X. Li, Z. Yao, Y. He, and S. Dai, "Modeling and experimental investigation of thermal–mechanical–electric coupling dynamics in a standing wave ultrasonic motor," *Smart Mater. Struct.*, vol. 26, no. 9, 2017, Art. no. 095044.
[39] Y. Liu, S. Shi, D. Wang, W. Chen, and D. Xu, "Research on the thermal characteristics of bending hybrid piezoelectric actuators under different exciting methods," *Ceramics Int.*, vol. 43, pp. S15–S20, Aug. 2017.
[40] F. Li, Z. Xu, X. Wei, and X. Yao, "Temperature- and DC bias field-dependent piezoelectric effect of soft and hard lead zirconate titanate ceramics," *J. Electroceramics*, vol. 24, no. 4, pp. 294–299, 2010.
[41] Q. Zhang, W. Chen, Y. Liu, J. Liu, and Q. Jiang, "A frog-shaped linear piezoelectric actuator using first-order longitudinal vibration mode," *IEEE Trans. Ind. Electron.*, vol. 64, no. 3, pp. 2188–2195, Mar. 2017.
[42] F. Zhang, W. Chen, J. Lin, and Z. Wang, "Bidirectional linear ultrasonic motor using longitudinal vibrating transducers," *IEEE Trans. Ultrason., Ferroelectr., Freq. Control*, vol. 52, no. 1, pp. 134–138, Jan. 2005.
[43] S. He, W. Chen, X. Tao, and Z. Chen, "Standing wave bi-directional linearly moving ultrasonic motor," *IEEE Trans. Ultrason., Ferroelectr., Freq. Control*, vol. 45, no. 5, pp. 1133–1139, Sep. 1998.
[44] W. Seemann, "A linear ultrasonic traveling wave motor of the ring type," *Smart Mater. Struct.*, vol. 5, no. 3, pp. 361–368, 1996.
[45] A. Iula, A. Corbo, and M. Pappalardo, "FE analysis and experimental evaluation of the performance of a travelling wave rotary motor driven by high power ultrasonic transducers," *Sens. Actuators A, Phys.*, vol. 160, pp. 94–100, May 2010.
[46] T. Peng, H. Shi, X. Liang, F. Luo, and X. Wu, "Experimental investigation on sandwich structure ring-type ultrasonic motor," *Ultrasonics*, vol. 56, pp. 303–307, Feb. 2015.
[47] W. Ou, M. Yang, F. Meng, Z. Xu, X. Zhuang, and S. Li, "Continuous high-performance drive of rotary traveling-wave ultrasonic motor with water cooling," *Sens. Actuators A, Phys.*, vol. 222, pp. 220–227, Feb. 2015.
[48] M. Kurosawa and S. Ueha, "High speed ultrasonic linear motor with high transmission efficiency," *Ultrasonics*, vol. 27, no. 1, pp. 39–44, 1989.
[49] T. Yokose, H. Hosaka, R. Yoshida, and T. Morita, "Resonance frequency ratio control with an additional inductor for a miniaturized resonant-type SIDM actuator," *Sens. Actuators A, Phys.*, vol. 214, pp. 142–148, Aug. 2014.
[50] Y. Liu, W. Chen, X. Yang, and J. Liu, "A rotary piezoelectric actuator using the third and fourth bending vibration modes," *IEEE Trans. Ind. Electron.*, vol. 61, no. 8, pp. 4366–4373, Aug. 2014.
[51] Y. Liu, J. Yan, L. Wang, and W. Chen, "A two-DOF ultrasonic motor using a longitudinal–bending hybrid sandwich transducer," *IEEE Trans. Ind. Electron.*, vol. 66, no. 4, pp. 3041–3050, Apr. 2019, doi: 10.1109/TIE.2018.2847655.
[52] S. Shi, H. Xiong, Y. Liu, W. Chen, and J. Liu, "A ring-type multi-DOF ultrasonic motor with four feet driving consistently," *Ultrasonics*, vol. 76, pp. 234–244, Apr. 2017.
[53] X. Yang, Y. Liu, W. Chen, and J. Liu, "Sandwich-type multi-degree-of-freedom ultrasonic motor with hybrid excitation," *IEEE Access*, vol. 4, pp. 905–913, 2016.
[54] Y. Liu, W. Chen, J. Liu, and S. Shi, "A high-power linear ultrasonic motor using longitudinal vibration transducers with single foot," *IEEE Trans. Ultrason., Ferroelectr., Freq. Control*, vol. 57, no. 8, pp. 1860–1867, Aug. 2010.
[55] Y. Liu, J. Liu, W. Chen, and S. Shi, "A u-shaped linear ultrasonic motor using longitudinal vibration transducers with double feet," *IEEE Trans. Ultrason., Ferroelectr., Freq. Control*, vol. 59, no. 5, pp. 981–989, May 2012.
[56] P. E. Tenzer and R. B. Mrad, "A systematic procedure for the design of piezoelectric inchworm precision positioners," *IEEE/ASME Trans. Mechatronics*, vol. 9, no. 2, pp. 427–435, Jun. 2004.
[57] Z. Chen, X. Li, P. Ci, G. Liu, and S. Dong, "A standing wave linear ultrasonic motor operating in in-plane expanding and bending modes," *Rev. Sci. Instrum.*, vol. 86, no. 3, 2015, Art. no. 035002.
[58] O. Vyshnevsky, S. Kovalev, and W. Wischnewskiy, "A novel, single-mode piezoceramic plate actuator for ultrasonic linear motors," *IEEE Trans. Ultrason., Ferroelectr., Freq. Control*, vol. 52, no. 11, pp. 2047–2053, Nov. 2005.
[59] Y. Shi, Y. Li, C. Zhao, and J. Zhang, "A new type butterfly-shaped transducer linear ultrasonic motor," *J. Intell. Mater. Syst. Struct.*, vol. 22, no. 6, pp. 567–575, 2011.
[60] B. Zhang, Z. Yao, Z. Liu, and X. Li, "A novel L-shaped linear ultrasonic motor operating in a single resonance mode," *Rev. Sci. Instrum.*, vol. 89, no. 1, 2018, Art. no. 015006.

WEISHAN CHEN was born in Laoting, China, in 1965. He received the B.E. and M.E. degrees in precision instrumentation engineering and the Ph.D. degree in mechatronics engineering from the Harbin Institute of Technology, China, in 1986, 1989, and 1997, respectively. Since 1999, he has been a Professor with the School of Mechatronics Engineering, Harbin Institute of Technology. His research interests include ultrasonic driving, smart materials and structures, and bio-robotics.

XINQI TIAN was born in Inner Mongolia, China, in 1992. He received the B.E. and M.E. degrees from the School of Mechatronics Engineering, Harbin Institute of Technology, China, in 2014 and 2016, respectively, where he is currently pursuing the Ph.D. degree. His research interests include ultrasonic motor and precision piezoelectric actuating.

SHUO CHEN was born in Laoting, China, in 1991. He received the B.E. degree in mechanical design, manufacturing and automation and the M.E. degree in mechatronics engineering from the School of Mechatronics Engineering, Harbin Engineering University, China, in 2014 and 2017, respectively. He is currently pursuing the Ph.D. degree in control science and engineering with the Harbin Institute of Technology, China. His research interests include precision piezoelectric actuating and control, spacecraft attitude control sensing, and actuator implementation.

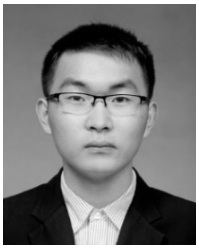

KAILEI XUE was born in Nantong, China, in 1994. He received the B.E. and M.E. degrees from the School of Mechatronics Engineering, Harbin Institute of Technology, China, in 2016 and 2018, respectively. His research interests include ultrasonic motor, piezoelectric actuating, and precision actuating.

HONGPENG YU was born in Mudanjiang, China, in 1996. He received the B.E. degree from the School of Mechatronics Engineering, Harbin Institute of Technology, China, in 2017, where he is currently pursuing the Ph.D. degree. His research interests include piezoelectric actuators and ultrasonic motors.